

Short Note

5-((3',5'-Dibromo-[2,2'-bithiophen]-5-yl)methyl)-3-ethyl-2-thioxothiazolidin-4-one·Br₂ (1:1)

Enrico Podda^{1,2,*}, Simone Acca¹, Maria Carla Aragoni¹, Vito Lippolis¹, Anna Pintus¹,
Massimiliano Arca¹ and Giuseppe Sforazzini^{1,*}

¹ Dipartimento di Scienze Chimiche e Geologiche, Università degli Studi di Cagliari, S.S. 554 Bivio Sestu, 09042 Monserrato, Italy

² Centro Servizi di Ateneo per la Ricerca (CeSAR), Università degli Studi di Cagliari, S.S. 554 Bivio Sestu, 09042 Monserrato, Italy

* Correspondence: enrico.podda@unica.it (E.P.); giuseppe.sforazzini@unica.it (G.S.)

Abstract

The reaction of rhodanine vinyl bithiophene (BTR) with molecular dibromine (Br₂) resulted in the formation of compound **1**. Single-crystal X-ray diffraction analysis revealed bromination of the terminal thiophenyl ring and the formation of a 1:1 CT “spoke” adduct between the rhodanine thiocarbonyl group and a neutral dibromine (Br₂) molecule.

Keywords: bithiophene; rhodanine; halogen bonding; SC-XRD

1. Introduction

π -Conjugation plays a pivotal role in the design and development of advanced functional materials with applications across materials science, including electronics, photonics, and sensing technologies. It critically influences the supramolecular organization of small molecules and underpins the development of organic electronic devices such as lasers, solar cells, transistors, and light-emitting diodes (LEDs) [1–3]. Additionally, π -conjugation is recognized as a key factor in the performance of photonic materials, including single-crystal optical waveguides [4,5].

Among the diverse classes of π -conjugated systems, thiophene and its derivatives represent some of the most widely employed building blocks. These compounds have found widespread use in pharmaceuticals [6], organic electronics [7], and luminescent materials [8]. The self-assembly of π -conjugated small molecules is not solely governed by hydrophobic interactions such as π - π stacking but is also significantly influenced by different non-covalent interactions (NCIs), including hydrogen bonding (HB) [9,10], halogen bonding (HaB) [11,12], and chalcogen bonding (ChB) [13,14]. These highly directional forces belong to the σ -hole interaction family and are named after the interacting atom with the region of positive electrostatic potential [15–17]. Therefore, the study of the reactivity between π -conjugated small molecules functionalized with chalcogenone groups and halogenated species is of particular interest; these synthons are ideal model systems for investigating the synergy and competition between various NCIs [17–19]. To better understand the cooperative or competitive interplay between NCIs in the molecular organization at the solid state, we recently explored the reactivity of rhodanine vinyl bithiophene (BTR) toward diiodine (I₂) (Scheme 1) [20]. This tecton was investigated as a model compound representing a typical terminal segment in organic π -conjugated small molecules for applications in optoelectronics. Interestingly, the CT “spoke” adduct with formula



Academic Editor: R. Alan Aitken

Received: 31 July 2025

Revised: 8 August 2025

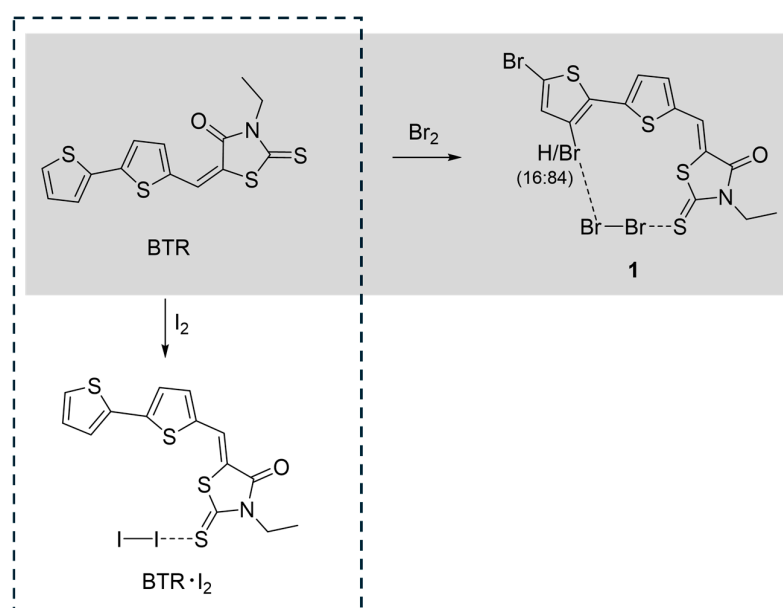
Accepted: 11 August 2025

Published: 14 August 2025

Citation: Podda, E.; Acca, S.; Aragoni, M.C.; Lippolis, V.; Pintus, A.; Arca, M.; Sforazzini, G. 5-((3',5'-Dibromo-[2,2'-bithiophen]-5-yl)methyl)-3-ethyl-2-thioxothiazolidin-4-one·Br₂ (1:1). *Molbank* **2025**, *2025*, M2047. <https://doi.org/10.3390/M2047>

Copyright: © 2025 by the authors. Licensee MDPI, Basel, Switzerland. This article is an open access article distributed under the terms and conditions of the Creative Commons Attribution (CC BY) license (<https://creativecommons.org/licenses/by/4.0/>).

BTR·I₂ was isolated, and its electrical conductivity was tested; the determination of its crystal structure allowed us to investigate its supramolecular architecture, arising from the interplay between π - π stacking interactions, ChBs, and HaBs.



Scheme 1. Reactivity of BTR towards I₂ and Br₂.

Following our previous report on the π -conjugated system BTR and its diiodine adduct BTR·I₂, we report our findings on the reactivity of BTR towards Br₂.

2. Results

BTR was synthesized in two steps, starting from commercially available 2,2'-bithiophene [20]. The first step involved a Vilsmeier–Haack reaction with phosphorus oxychloride (POCl₃) and dimethylformamide (DMF) in 1,2-dichloroethane (1,2-DCE), which afforded 2,2'-bithiophene-5-carbaldehyde in a quantitative yield. The resulting aldehyde intermediate then underwent Knoevenagel condensation with *N*-ethylrhodanine in the presence of piperidine and ethanol, yielding BTR in a quantitative yield. BTR was intentionally designed to fulfill the typical requirements of small-molecule (SM) semiconductors featuring a conjugated polycyclic core of bithiophene asymmetrically functionalized by an electron-deficient rhodanine group [21,22]. Another key feature of BTR is the presence of the thiocarbonyl C=S bond at the rhodanine. Chalcogenone derivatives (C=Ch; Ch=S, Se, and Te), in contrast to their carbonyl analogs, possess a strong affinity for dihalogens and display a broader chemistry. In fact, by reacting a dihalogen X₂ with chalcogenone donors (RE; E = S, Se, and Te; R = organic moiety), several types of products can theoretically be formed, namely linear “spoke” CT adducts, “T-shaped” products featuring the hypercoordinate chalcogen atom, halonium compounds (RE-X-RE)⁺, and different types of cationic oxidation products, such as dications (RE-RE)²⁺ [15]. CT “spoke” adducts and hypercoordinate “T-shaped” compounds exhibit linear three-body systems: X-X-E in the former case and X-E-X in the latter. The preferential formation of one product over another depends on several factors, including the oxidation strength of the dihalogens and the solvent employed [15]. As mentioned above, we investigated the reactivity of BTR with I₂, observing the formation of the BTR·I₂ CT adduct, which was confirmed by single-crystal X-ray diffraction [20]. BTR reacted with Br₂ in a 1:2 molar ratio using acetonitrile as the solvent. After 72 h, red block-shaped crystals of compound 1 were obtained and structurally characterized by single-crystal X-ray diffraction (Tables S1–S3).

Structural characterization revealed that the product consists of a 1:1 CT “spoke” adduct of the dibrominated BTR ligand (BTR’). Bromination occurred at positions 3 and 5 of the terminal thiophene ring (Figure 1). While position 5 is the most reactive towards bromination (featuring a more negative natural charge, $-0.416 |e|$, as computed through DFT calculations; see Materials and Methods for details), the disubstitution of thiophenes at positions 3 and 5 is uncommon [23]. Accordingly, a model was built to describe the partial occupancy of H and Br at position 3 of the terminal thiophenyl ring, indicating a 16% contribution of monobromination (H in position 3 and Br in position 5) and an 84% contribution of dibromination (Br in positions 3 and 5).

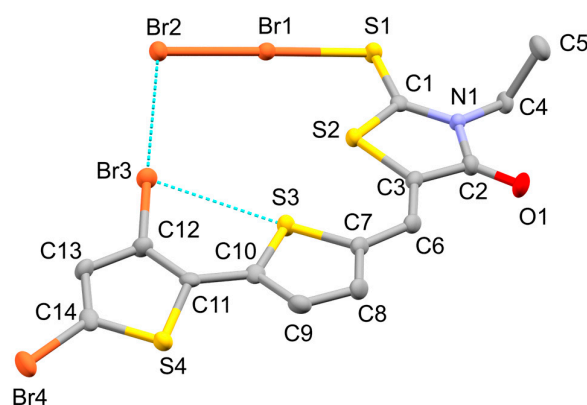


Figure 1. X-ray crystal structure of compound BTR’·Br₂ (**1**) with the numbering scheme adopted viewed along the *b*-axis. Displacement ellipsoids are drawn at a 50% probability level. H atoms have been omitted for clarity. Br3···Br2, 3.5877(9) Å; C12-Br3, 1.881(5) Å; C12-Br3···Br2, 177.8(2)°. Crystal data for compound **1**: C₁₄H_{9.16}Br_{3.84}NOS₄, (*M_r* = 642.48 g mol⁻¹) triclinic, *P*-1, *a* = 8.5467(9) Å, *b* = 9.6336(10) Å, *c* = 12.2630(11) Å, α = 84.742(4)°, β = 75.994(4)°, γ = 75.733(5)°, *V* = 948.90(17) Å³, *T* = 100(2) K, *Z* = 2, ρ_{calc} = 2.249 g/cm³, $\mu(\text{Mo } K\alpha)$ = 8.588 mm⁻¹. The final *R*₁ value was 0.0462 [*F*² ≥ 2 σ (*F*²)], *wR*₂ was 0.0880 (all data), and GooF = 1.050.

The thiocarbonyl group of BTR’ interacts with a Br₂ unit to form the 1:1 CT adduct BTR’·Br₂ (**1**) featuring a linear (C=S)-Br-Br moiety [S1-Br1, 2.4512(16); Br1-Br2, 2.5257(8) Å; S1-Br1-Br2, 176.71(5)°]. It is noteworthy that CT adducts involving a S-Br-Br moiety, where all distances fall within the range of covalent bonds, are quite uncommon, with only six examples found in the CCDC (ConQuest 2025 1.1.) [24–27]. The S-Br and Br-Br distances for compound **1** are in line with those found in other CT adducts previously reported. For example, the geometrical parameters observed for the (C=S)-Br-Br moiety in the crystal structure of [(2(3*H*)-benzothiazolethione)Br₂] (refcode JOXGEK; see ref. [25]) are S1-Br1, 2.283(2); Br1-Br2, 2.814(1) Å; and S1-Br1-Br2, 175.33(4)°. This indicates slightly stronger interactions compared to that observed for compound **1**. The S-Br-Br fragment falls in the correlation developed for linear three-body systems from structural data (red dot in Figure S1) [28].

Considering the major component (see the experimental section for details), corresponding to the dibrominated species BTR’, the molecule exhibits a non-planar geometry: the terminal thiophene and rhodanine moieties are twisted by 12° and 8°, respectively, with respect to the central thiophenyl ring (Figure 2a and Figure 2b, respectively).

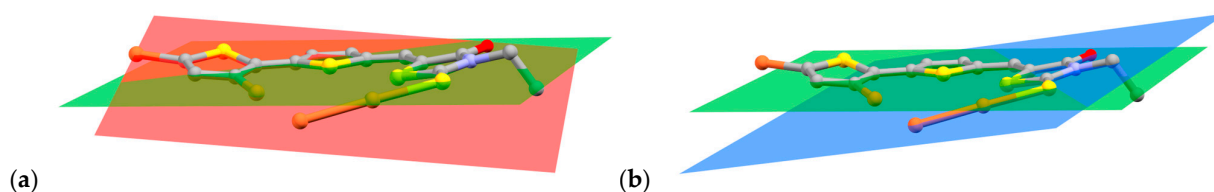


Figure 2. Perspective views of the conformation adopted by **1** showing the intersections between the planes described over the central thiophene (green) and (a) the terminal thiophene (red) and (b) rhodanine (blue) moieties.

The observed deviation from planarity results from a weak intramolecular halogen bond (HaB) with the bromine Br2 atom acting as the HaB acceptor [Br3⋯Br2, 3.5877(9) Å, C12-Br3, 1.881(5) Å, C12-Br3⋯Br2, 177.8(2)°, Figure 3]. This HaB, along with an intramolecular ChB of the type C-S⋯Br [S3⋯Br3 = 3.241(2); C7-S3 = 1.732(6) Å; C7-S3⋯Br3 = 170.1(2)°], cooperatively stabilize the *pseudo*-antiperiplanar conformation of the two thiophenyl rings in compound **1** (Figure 3).

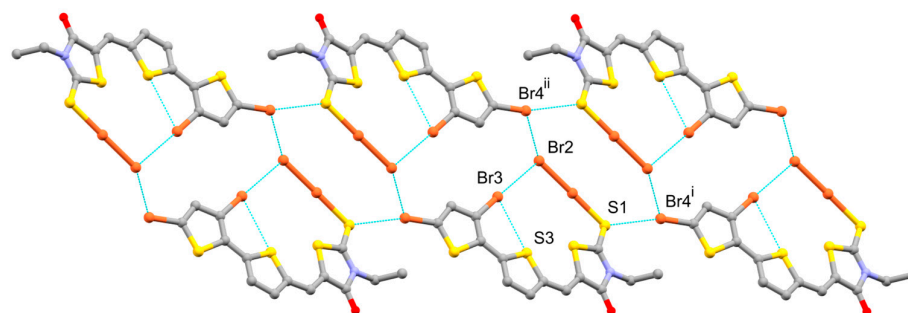


Figure 3. View of the NCIs found in **1** along the *b*-axis. $^i = -1 + x, 1 + y, 1 + z$; $^{ii} = 1 - x, 1 - y, -z$.

This is in contrast to the previously reported crystal structure of BTR, where the molecule was found to be planar (excluding the aliphatic pendant arm). Notably, planarity was also retained in the CT “spoke” adduct BTR·I₂. [20] This suggests that bromination and the subsequent formation of HaB and ChB are responsible for the twisted conformation observed in compound **1**. The thiocarbonyl sulfur atom S1 is engaged in an additional HaB with the symmetry-related Br4 atom, with a S1⋯Br4ⁱ ($^i = -1 + x, 1 + y, 1 + z$) distance of 3.427(2) Å, which is shorter than the sum of the atomic van der Waals radii (3.65 Å) [29]. These interactions generate 1D chains running parallel to the $[\bar{1}11]$ direction. Finally, a weak HaB (3.690 Å) is formed between the terminal Br2 atom and the C14ⁱⁱ-Br4ⁱⁱ group of a symmetry-related molecular unit (Figure 3). The pattern of inter- and intramolecular contacts aligns with the Potential Electrostatic Map (MEP) calculated for compound **1** (Figure 4), which clearly shows the σ -holes located on the Br2 and Br4 atoms.

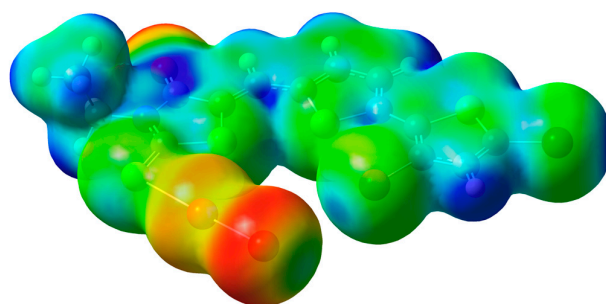


Figure 4. Molecular electrostatic potential (MEP) mapped on the electron density [$5 \cdot 10^{-3} |e|/\text{Bohr}^3$; range -0.040 (red) to $+0.007$ (blue) a.u.] calculated for compound **1** at the DFT level.

3. Materials and Methods

3.1. General

BTR was synthesized as previously reported [20]. Elemental analysis determinations were performed with a Perkin Elmer EA CHN elemental analyzer (Shelton, CT, USA). The FT-IR spectra ($4000\text{--}400\text{ cm}^{-1}$) were recorded using KBr pellets on a Thermo Nicolet 5700 spectrometer (Waltham, MA, USA). Melting point determination was performed on a FALC mod. C apparatus. Single-crystal X-ray diffraction data for compound **1** were collected on a Bruker D8 Venture diffractometer (Karlsruhe, Germany) at 100 K using ω scans. Structure solution was carried out by using SHELXT [30] implemented in Olex2 [31], which readily identified the space group $P - 1$ and provided a correct assignment for all non-hydrogen atoms. Initial refinement using full-matrix least-squares minimization on F^2 with ShelXL [32] converged at $R1 \approx 7.5\%$, which improved to 5.7% upon applying anisotropic displacement parameters to all non-H atoms. Inspection of the residual electron density map revealed a significant peak (2.2 e \AA^{-3}) located in proximity to the 3-position of the terminal thiophenyl ring, suggesting partial bromination (Br3 in Figure 1). Therefore, a model was introduced to account for the presence of two species (H/Br, H12/Br3) co-crystallized at the same site. The atomic occupancies were set so that they added up to 1, with a final ratio of 16:84 for H:Br, respectively. H-atoms were placed in calculated positions and refined isotropically using a riding model with $U_{\text{iso}}(\text{H}) = 1.2 U_{\text{eq}}(\text{C})$. The final model converged smoothly, yielding $R1 = 4.62\%$; an $wR2$ value of 8.80% ; and $\text{GooF} = 1.050$. A refinement model in which Br3 was treated with full occupancy led to significantly poorer refinement statistics ($R1 = 5.59$; $wR2 = 12.90$), along with larger residual electron density peaks (max peak = 1.5 ; min peak = -2.2 e \AA^{-3}). These findings support the initial interpretation of the structure as a co-crystallization of two components, with a refined Br3 occupancy of 84% yielding the best fit to the experimental data. DFT [33,34] calculations were carried out both on BTR and compound **1** at the DFT level with the commercial suite of programs Gaussian 16 [35] by adopting the mPW1PW hybrid functional [36]. The def2-TZVP basis set [37,38] was adopted for all atomic species. The memory required for each calculation was evaluated by the GaussMem cross-platform (Linux, macOS, Windows) program as a function of the number of shared processors, the total number of basis set functions, and a memory threshold depending on the highest angular momentum basis function [39]. The nature of the minima of each optimized geometry was verified by harmonic frequency calculations. Natural charge distributions were evaluated at the NBO level [40] at the optimized geometries. The program GaussView 6.1.1 [41] was used to investigate the optimized structures, the NBO charges, and the MEPs.

3.2. Synthesis of Compound **1**

BTR (10.2 mg ; $3.0 \times 10^{-5}\text{ mol}$) was dissolved in 3 mL of acetonitrile, and 2.4 mL of a 0.025 M Br_2 solution ($6.0 \times 10^{-5}\text{ mol}$) in the same solvent was added dropwise. The resulting solution was stored at $4\text{ }^\circ\text{C}$ for 72 h . Red block-shaped crystals of the product were separated from the solution and air-dried (8.3 mg ; 42%). For structural characterization, crystals of **1** were harvested directly from the mother liquor and dispersed in perfluoroether oil. A suitable crystal was selected and mounted on a MiTeGen loop before being analyzed through the SC-XRD routine. Elemental analysis calcd (%) for $\text{C}_{14}\text{H}_{9.16}\text{Br}_{3.84}\text{NOS}_4$: C 26.17 , H 1.44 , N 2.18 . Found: C 26.25 , H 1.27 , N 2.25 . m.p. = $179\text{ }^\circ\text{C}$ dec. FT-IR (KBr, $4000\text{--}400\text{ cm}^{-1}$): 3085 w , 2918 s , 2850 ms , 1699 vs , 1583 s , 1434 s , 1384 m , 1322 m , 1240 ms , 1130 ms , 788 w , 613 w , 519 w cm^{-1} .

4. Conclusions

The reaction between BTR and Br₂ in acetonitrile afforded compound **1**, which was isolated and characterized. SC-XRD analysis of crystals of **1** revealed the formation of a charge transfer (CT) “spoke” adduct in which the thiocarbonyl chalcogen atom interacts with a neutral dibromine molecule. In addition, bromination occurred at positions 3 and 5 of the terminal thiophene. A network of both intra- and intermolecular NCIs, including HaBs and ChBs, was also observed. In summary, the ability of BRT to produce CT adducts through the thiocarbonyl group of the rhodanine (Lewis basicity) and undergo bromination on the bithiophene moiety demonstrates its versatility as a reagent for designing supramolecular solid-state frameworks based on HaB and ChB interactions. In this context, we are currently investigating the reactivity of dihalogens and interhalogens towards a wide range of different polythiophene derivatives differing in size and shape, as well as in the number and directionality of the terminal thiocarbonyl groups, in order to use these building blocks in the rational construction of novel solid-state architectures.

Supplementary Materials: The following supporting information can be downloaded online. Figure S1: Structural data of linear S-X-Y fragments deposited at the CSD reported as scatter plot of the S...X and X...Y relative distances. Figure S2: FT-IR spectrum of compound **1**. Table S1: Crystal data and refinement parameters for compound **1**. Table S2: Bond lengths (Å) for compound **1**. Table S3: Bond angles (°) for compound **1**. Table S4: Orthogonal Cartesian coordinates for BTR at the DFT-optimized geometry (mPW1PW/def2TZVP). Table S5: Orthogonal Cartesian coordinates for compound **1** at the DFT-optimized geometry (mPW1PW/def2TZVP).

Author Contributions: Conceptualization: G.S., M.A. and E.P. Data curation: M.C.A., E.P., A.P. and M.A. Investigation: S.A., M.C.A., V.L., A.P., E.P. and M.A. Writing (original draft): E.P. and G.S. All authors have read and agreed to the published version of the manuscript.

Funding: We thank the Ministero per l’Ambiente e la Sicurezza Energetica (MASE; formerly Ministero della Transizione Ecologica, MITE)—Direzione generale Economia Circolare (RAEE - Edizione 2021; “Recupero Selettivo Sostenibile Metalli RAEE”) and Fondazione di Sardegna (FdS Progetti Biennali di Ateneo, annualità 2022, F73C23001580007).

Data Availability Statement: Crystallographic data were deposited at CCCD with deposition number 2475848.

Acknowledgments: We acknowledge the CeSAR (Centro Servizi di Ateneo per la Ricerca) of the University of Cagliari, Italy, for providing access to the SC-XRD facility.

Conflicts of Interest: The authors declare no conflicts of interest.

References

1. Sawatzki-Park, M.; Wang, S.; Kleemann, H.; Leo, K. Highly Ordered Small Molecule Organic Semiconductor Thin-Films Enabling Complex, High-Performance Multi-Junction Devices. *Chem. Rev.* **2023**, *123*, 8232–8250. [[CrossRef](#)]
2. Fratini, S.; Nikolka, M.; Salleo, A.; Schweicher, G.; Sirringhaus, H. Charge transport in high-mobility conjugated polymers and molecular semiconductors. *Nat. Mater.* **2020**, *19*, 491–502. [[CrossRef](#)]
3. Chen, J.; Zhang, W.; Wang, L.; Yu, G. Recent Research Progress of Organic Small-Molecule Semiconductors with High Electron Mobilities. *Adv. Mater.* **2023**, *35*, 2210772. [[CrossRef](#)] [[PubMed](#)]
4. Tian, D.; Chen, Y. Optical Waveguides in Organic Crystals of Polycyclic Arenes. *Adv. Opt. Mater.* **2021**, *9*, 2002264. [[CrossRef](#)]
5. Podda, E.; Arca, M.; Pintus, A.; Lippolis, V.; Coles, S.J.; Orton, J.B.; Porcu, S.; Ricci, P.C.; Aragoni, M.C. Ultra-Low Optical Loss in Single Crystal Waveguides of Fluorene/Fluorenone Cd^{II} Coordination Polymers. *JACS Au* **2025**, *5*, 727–739. [[CrossRef](#)]
6. Gramec, D.; Peterlin Mašič, L.; Sollner Dolenc, M. Bioactivation Potential of Thiophene-Containing Drugs. *Chem. Res. Toxicol.* **2014**, *27*, 1344–1358. [[CrossRef](#)]
7. Perepichka, I.F.; Perepichka, D.F. (Eds.) *Handbook of Thiophene-Based Materials: Applications in Organic Electronics and Photonics*; Wiley-VCH: Weinheim, Germany, 2009; Volume 1–2, ISBN 978-0-470-05732-2.

8. Podda, E.; Coles, S.J.; Horton, P.N.; Lickiss, P.D.; Bull, O.S.; Orton, J.B.; Pintus, A.; Pugh, D.; Aragoni, M.C.; Davies, R.P. First Example of Solid-State Luminescent Borasiloxane-Based Chiral Helices Assembled through N–B Bonds. *Dalton Trans.* **2021**, *50*, 3782–3785. [[CrossRef](#)]
9. Arunan, E.; Desiraju, G.R.; Klein, R.A.; Sadlej, J.; Scheiner, S.; Alkorta, I.; Clary, D.C.; Crabtree, R.H.; Dannenberg, J.J.; Hobza, P.; et al. Definition of the hydrogen bond (IUPAC Recommendations 2011). *Pure Appl. Chem.* **2011**, *83*, 1637–1641. [[CrossRef](#)]
10. Steiner, T. The Hydrogen Bond in the Solid State. *Angew. Chem. Int. Ed. Engl.* **2002**, *41*, 48–76. [[CrossRef](#)]
11. Desiraju, G.R.; Ho, P.S.; Kloo, L.; Legon, A.C.; Marquardt, R.; Metrangolo, P.; Politzer, P.; Resnati, G.; Rissanen, K. Definition of the halogen bond (IUPAC Recommendations 2013). *Pure Appl. Chem.* **2013**, *85*, 1711–1713. [[CrossRef](#)]
12. Cavallo, G.; Metrangolo, P.; Milani, R.; Pilati, T.; Priimagi, A.; Resnati, G.; Terraneo, G. The Halogen Bond. *Chem. Rev.* **2016**, *116*, 2478–2601. [[CrossRef](#)]
13. Aakeröy, C.B.; Bryce, D.L.; Desiraju, G.R.; Frontera, A.; Legon, A.C.; Nicotra, F.; Rissanen, K.; Scheiner, S.; Terraneo, G.; Metrangolo, P.; et al. Definition of the chalcogen bond (IUPAC Recommendations 2019). *Pure Appl. Chem.* **2019**, *91*, 1889–1892. [[CrossRef](#)]
14. Vogel, L.; Wonner, P.; Huber, S.M. Chalcogen Bonding: An Overview. *Angew. Chem. Int. Ed.* **2019**, *58*, 1880–1891. [[CrossRef](#)]
15. Podda, E.; Arca, M.; Aragoni, M.C.; Caltagirone, C.; Lippolis, V.; Pintus, A.; Paixão, D.B.; Soares, E.G.O.; Schneider, P.H. Synergistic Interplay between Intermolecular Halogen and Chalcogen Bonds in the Dihalogen Adducts of 2,5-Bis(Pyridine-2-Yl)Tellurophene: Reactivity Insights and Structural Trends. *Inorg. Chem.* **2025**, *64*, 10972–10988. [[CrossRef](#)]
16. Politzer, P.; Murray, J.S.; Clark, T.; Resnati, G. The σ -hole revisited. *Phys. Chem. Chem. Phys.* **2017**, *19*, 32166–32178. [[CrossRef](#)]
17. Politzer, P.; Murray, J.S. σ -hole Interactions: Perspectives and Misconception. *Crystals* **2017**, *7*, 212. [[CrossRef](#)]
18. Aragoni, M.C.; Arca, M.; Lippolis, V.; Pintus, A.; Torubaev, Y.; Podda, E. A Structural Approach to the Strength Evaluation of Linear Chalcogen Bonds. *Molecules* **2023**, *28*, 3133. [[CrossRef](#)]
19. Aragoni, M.C.; Cherchi, M.F.; Lippolis, V.; Pintus, A.; Podda, E.; Slawin, A.M.Z.; Woollins, J.D.; Arca, M. Self-Assembly of Supramolecular Architectures Driven by σ -Hole Interactions: A Halogen-Bonded 2D Network Based on a Diiminedibromido Gold(III) Complex and Tribromide Building Blocks. *Molecules* **2022**, *27*, 6289. [[CrossRef](#)]
20. Sanna, A.L.; Acca, S.; Podda, E.; Mascia, A.; Pintus, A.; Aragoni, M.C.; Lippolis, V.; Ricci, C.; Cosseddu, P.; Arca, M.; et al. Unveiling the significance of adduct formation between thiocarbonyl Lewis donors and diiodine for the structural organization of rhodanine-based small molecule semiconductors. *J. Mater. Chem. C* **2024**, *12*, 11352–11360. [[CrossRef](#)]
21. Yi, J.; Zhang, G.; Yu, H.; Yan, H. Advantages, challenges and molecular design of different material types used in organic solar cells. *Nat. Rev. Mater.* **2023**, *9*, 46–62. [[CrossRef](#)]
22. Li, X.; Kong, X.; Sun, G.; Li, Y. Organic small molecule acceptor materials for organic solar cells. *eScience* **2023**, *3*, 100171. [[CrossRef](#)]
23. Fröhlich, H.; Kalt, W. Base-Catalyzed Halogen Dance Reaction at Thiophenes: A Spectroscopic Reinvestigation of the Synthesis of 2,5-Dibromo-3-(trimethylsilyl)thiophene. *J. Org. Chem.* **1990**, *55*, 2993–2995. [[CrossRef](#)]
24. Saab, M.; Nelson, D.J.; Leech, M.C.; Lam, K.; Nolan, S.P.; Nahra, F.; Van Hecke, K. Reactions of *N*-heterocyclic carbene-based chalcogenoureas with halogens: A diverse range of outcomes. *Dalton Trans.* **2022**, *51*, 3721–3733. [[CrossRef](#)]
25. Koskinen, L.; Jääskeläinen, S.; Hirva, P.; Haukka, M. Tunable Interaction Strength and Nature of the S \cdots Br Halogen Bonds in [(Thione)Br₂] Systems. *Cryst. Growth Des.* **2015**, *15*, 1160–1167. [[CrossRef](#)]
26. Vaughan, G.B.M.; Mora, A.J.; Fitch, A.N.; Gates, P.N.; Muir, A.S. A high resolution powder X-ray diffraction study of the products of reaction of dimethyl sulfide with bromine; crystal and molecular structures of (CH₃)₂SBr_n (*n* = 2, 2.5 or 4). *J. Chem. Soc. Dalton Trans.* **1999**, 79–84. [[CrossRef](#)]
27. Steinfeld, G.; Lozan, V.; Krüger, H.J.; Kersting, B. Trapping of a Thiolate \rightarrow Dibromine Charge-Transfer Adduct by a Macrocyclic Dinickel Complex and Its Conversion into an Arenesulfonyl Bromide Derivative. *Angew. Chem. Int. Ed.* **2009**, *48*, 1954–1957. [[CrossRef](#)] [[PubMed](#)]
28. Aragoni, M.C.; Arca, M.; Devillanova, F.A.; Isaia, F.; Lippolis, V. Adducts of S/Se Donors with Dihalogens as a Source of Information for Categorizing the Halogen Bonding. *Cryst. Growth Des.* **2012**, *12*, 2769–2779. [[CrossRef](#)]
29. Bondi, A. van der Waals Volumes and Radii. *J. Phys. Chem.* **1964**, *68*, 441–451. [[CrossRef](#)]
30. Sheldrick, G.M. SHELXT-Integrated Space-Group and Crystal-Structure Determination. *Acta Cryst. A* **2015**, *71*, 3–8. [[CrossRef](#)]
31. Dolomanov, O.V.; Bourhis, L.J.; Gildea, R.J.; Howard, J.A.K.; Puschmann, H. OLEX2: A Complete Structure Solution, Refinement and Analysis Program. *J. Appl. Cryst.* **2009**, *42*, 339–341. [[CrossRef](#)]
32. Sheldrick, G.M. Crystal Structure Refinement with SHELXL. *Acta Cryst. C* **2015**, *71*, 3–8. [[CrossRef](#)]
33. Koch, W.; Holthausen, M.C. *A Chemist's Guide to Density Functional Theory*; Wiley-VCH: New York, NY, USA, 2001; ISBN 978-3-527-30372-4.
34. Geerlings, P.; De Proft, F.; Langenaeker, W. Conceptual Density Functional Theory. *Chem. Rev.* **2003**, *103*, 1793–1874. [[CrossRef](#)]
35. Frisch, M.J.; Trucks, G.W.; Schlegel, H.B.; Scuseria, G.E.; Robb, M.A.; Cheeseman, J.R.; Scalmani, G.; Barone, V.; Petersson, G.A.; Nakatsuji, H.; et al. *Gaussian 16 (Rev. B01)*; Gaussian, Inc.: Wallingford, CT, USA, 2016.
36. Adamo, C.; Barone, V. Exchange functionals with improved long-range behavior and adiabatic connection methods without adjustable parameters: The mPW and mPW1PW models. *J. Chem. Phys.* **1998**, *108*, 664–675. [[CrossRef](#)]

37. Weigend, F.; Ahlrichs, R. Balanced basis sets of split valence, triple zeta valence and quadruple zeta valence quality for H to Rn: Design and assessment of accuracy. *Phys. Chem. Chem. Phys.* **2005**, *7*, 3297–3305. [[CrossRef](#)]
38. Weigend, F. Accurate Coulomb-fitting basis sets for H to Rn. *Phys. Chem. Chem. Phys.* **2006**, *8*, 1057–1065. [[CrossRef](#)]
39. Arca, M. GaussMem. 2024. Available online: <https://massimiliano-arca.itich.io/gaussmem> (accessed on 15 July 2025).
40. Reed, A.E.L.; Curtis, L.A.; Weinhold, F. Intermolecular Interactions from a Natural Bond Orbital, Donor-Acceptor View-point. *Chem. Rev.* **1988**, *88*, 899–926. [[CrossRef](#)]
41. Dennington, R.; Keith, T.A.; Millam, J.M. *GaussView, Version 6*; Semichem Inc.: Shawnee Mission, KS, USA, 2016.

Disclaimer/Publisher’s Note: The statements, opinions and data contained in all publications are solely those of the individual author(s) and contributor(s) and not of MDPI and/or the editor(s). MDPI and/or the editor(s) disclaim responsibility for any injury to people or property resulting from any ideas, methods, instructions or products referred to in the content.